*Thermochimica Acta*, 234 (1994) 53–83
Elsevier Science B.V., Amsterdam
*SSDI* 0040-6031(93)01520-D



# Mechanistic aspects of the reaction between carbon and oxygen [1]

B. Henschke, H. Schubert, J. Blöcker, F. Atamny and R. Schlögl *

*Institut für Anorganische Chemie der Universität Frankfurt, Marie-Curie Strasse 11, D-60439 Frankfurt (Germany)*

(Received 4 August 1993; accepted 27 August 1993)

**Abstract**

The nominally simple reaction between carbon in its graphitic modifications and molecular oxygen involves a complex sequence of reactions some of which are controlled by the topochemistry of the substrate. The paper presents attempts to characterise the initial carbon surface and is modifications during burn-off by chemical and spectroscopic techniques. Analysis of the topochemical aspect requires knowledge of the microscopic surface structure of, in particular, defective sections. Scanning tunnelling microscopy (STM) can give some insights into the local surface structure of partly reacted graphitic materials. Local electronic anomalies at step edges detected in STM are in agreement with their special reactivity postulated in models of the reaction mechanism.

## INTRODUCTION

The reaction between special samples of graphitic carbon and molecular oxygen is one facet of the scientific activities of the laureate of this special volume [1]. The analytical value of the oxidation kinetics of carbon in various microstructural modifications is stressed in his work. The underlying principle is the topotactic reaction control in the overall process. The reaction kinetics are not only a superposition of isotropic elementary reactions but are also severely affected by the geometric, and hence electronic, local anisotropy of the carbon substrate. In this way the shape of the basic structural units [2] (ratio of basal to prismatic faces) as well as the basal defect structure [3] exert control over rate and selectivity of the oxidation reaction. As many influences are superimposed into the observable reaction kinetics no straightforward separation is possible between electronic and geometric factors.

In our group an approach is taken [4] to try and understand qualitatively and quantitatively the elementary reaction steps in order to arrive at a

* Corresponding author.

[1] Dedicated to Hans Georg Wiedemann.

validated kinetic model with suitable adaptions for the topotactic characteristics of each type of carbon material. This attempt is not original to our group [5], the decisive influence of the surface topography on the reaction behaviour having long been well known [6] in kinetic models describing the overall oxidation [7]. The fundamental work in this area is compiled in a detailed review [8]. We use a combination of chemical and physical analytical techniques to investigate a variety of aspects of these complex reactions under comparable conditions in order to construct, experimentally, a qualitative picture of the reaction details. In a later step this picture will allow the formulation of a kinetic model with a selection of elementary steps based on experimental observations. The purpose of the present paper is to give a status report along this way.

A sequence of necessary elementary reactions may be written as follows:

$$C^* + O_2 \rightarrow C(O_2)_{ads} \quad (1)$$

$$C^* + C(O_2)_{ads} \rightarrow 2C(O) \quad (2)$$

$$C(O) + C_{def} \rightarrow C\text{–}O + C^* \quad (3)$$

$$C\text{–}O + C(O) \rightarrow CO_2 + C^* \quad (4)$$

Reactions (1) and (2) describe the activation of molecular oxygen occurring on reductive sites (C*) of graphitic surfaces via intermediate donation of $\pi$ electrons to yield molecular anionic intermediates [4] and finally chemisorbed oxygen atoms [C(O)]. Driven by the excess bond dissociation energy, the atoms will diffuse on the perfect basal plane of a graphene layer to find a defect ($C_{def}$). At this reaction site a covalent C–O bond will be formed (step (3)) which can desorb under conditions favouring very rapid oxidation and which will be oxidised to the final product $CO_2$ (step (4)) under kinetic conditions allowing total oxidation of the carbon.

Electronic factors as well as topotactic factors will control steps (1) and (2), solely topochemical properties of the substrate will control step (3) and external parameters as well as the factors affecting the production of C(O) will control step (4). These simple ideas illustrate the interplay of many possible influences on the rate law. The external parameters can be kept constant during reaction, but the topochemistry may change as a function of burn-off, if the defect distribution in the sample allows for a change in geometry of the oxidising particle. In this case the kinetic "constants" are not constant but become functions of the burn-off, precluding any meaningful macrokinetic analysis of the whole reaction. In consideration of these facts a detailed picture of the reaction will help to estimate the relative weight of possible influences on the reaction rate in order to simplify the model, which would otherwise have to consider a meaningless large number of adjustable parameters if all influences are to be considered explicitly.

In the present paper the following aspects of the large number of possible

variables in the overall kinetics will be considered: the state of the original surface in air at 300 K; thermal desorption of surface functional groups; chemisorption of oxygen; electronic structure of the reacting surface; microstructure of the carbon surface.

The materials in this study were chosen such as to approach real carbon matter (coal, soot) on the one hand to allow defined experiments with model graphite surfaces on the other. Industrial carbon blacks were found to be suitable test materials with the advantage of bulk availability with constant average properties over large sample batches. The natural graphite was kindly denoted by Graphitwerke Kropfmühl and the carbon blacks were provided by Degussa AG (Hanau).

## EXPERIMENTAL

The surface areas were determined from nitrogen adsorption isotherms following the Brunnaes–Emett–Teller (BET) analysis. Characteristic data of the various carbons used are collected in Table 1. Extraction of chemisorbed organics from the carbon black samples was carried out with toluene in a soxhlet extractor for 24 h.

X-ray diffraction was carried out with a Stoe Stadi P instrument in focussing Debye–Scherrer geometry with monochromated Cu radiation and a high resolution parallel detection system.

Surface titrations were carried out under exclusion of oxygen as well in the gas phase and in thrice distilled water. Chemisorption kinetics were determined and found to be in the steady state after 24 h of reaction. The acid–base titrations were carried out with an automatic titration processor from Metrohm.

Temperature programmed desorption (TPD) and temperature programmed reaction (TPR) experiments were carried out in a UHV system of laboratory manufacture equipped with a quadrupole mass spectrometer, a sample transfer device with low temperature specimen holder, a high pressure exposure system made from quartz glass and external heating

TABLE 1

Materials used

| | HOPG graphite [a] | RFL graphite | FLA 101 | FW 1 |
|---|---|---|---|---|
| Type of carbon | Oriented graphite | Natural flakes | Channel black | Gas black |
| BET surface [b] | 0.01 | 0.1 | 23.0 | 268.0 |
| Particle size/mm | Single crsytal | 0.5–0.1 | Complex aggregates | Complex aggregates |
| C content/wt% | 99.9 | 99.9 | 98.92 | 94.3 |
| H content/wt% | – | – | 0.32 | 0.40 |
| N content/wt% | – | – | 0.27 | 0.17 |
| O content/wt% [c] | – | – | 0.50 | 6.00 |

[a] Highly oriented pyrolytic graphite (Union Carbide).

[b] In $m^2 g^{-1}$ after degassing at 760 K. [c] Difference to 100%.

system and a computer controller heater power supply, in order to achieve linear heating rates of usually 3 K $s^{-1}$ in the low temperature sample holder and 1 K $s^{-1}$ with the external quartz cell. Details of the instrument can be found elsewhere [9].

XANES and photoemission experiments were carried out with samples deposited on polycrystalline copper plates. A UHV system equipped with total and partial yield detectors, with a hemispherical electron energy analyser and with a high pressure preparation attachment for oxidation experiments was connected to the SX 700 II or HEPGM II beam lines at the BESSY synchrotron facility in Berlin. Energy scales were calibrated with the Cu *L*III edge and with the carbon 1 s photoemission line at 284.6 eV as secondary standard.

STM images were obtained in air with a commercial Aris 6100 instrument from Burleigh. Pt–Ir tips were used and the scan parameters were chosen such that they had no influence on the images displayed. Details, the procedure of sample preparation and artifact analysis are presented elsewhere [10].

## RESULTS AND DISCUSSION

### The original surface

The possibilities and limitations of spectroscopic analysis of carbon surfaces have been discussed in detail in a previous publication [4] using the same carbon materials as described in the present study. In particular, the discrimination of chemically different carbon–oxygen functional groups by electron microscopy is poor [11]. Better selectivity can be obtained from a conventional wet chemical titration analysis of the functional groups. Characteristic examples are shown in Fig. 1. The data were collected from two sample batches in order to illustrate the degree of reproducibility which can be achieved.

The shape of the curve indicates a saturation behaviour as expected for a surface reaction. Different carbon materials exhibit, however, rather different curves as shown in Fig. 1. In one case a superposition of two saturation curves can be seen indicating more than one type of chemisorption sites being present on either the basic or acidic side of the pK distribution of the surface hydroxyl groups. A numerical analysis reveals that the splitting of the isotherms in two components is present in all cases but due to widely varying abundancies of the corresponding species with varying expression in the curve shape. The analysis of the isotherms within the linearised Langmuir sorption model thus yields at least two different sorption constants $b$ for either acid or base neutralisation and we obtain abundancies of four different oxygen functional groups. The chemical assignment [12] of these four types of groups is represented in Fig. 2.

The effect of admitting oxygen during chemisorption in aqueous solution

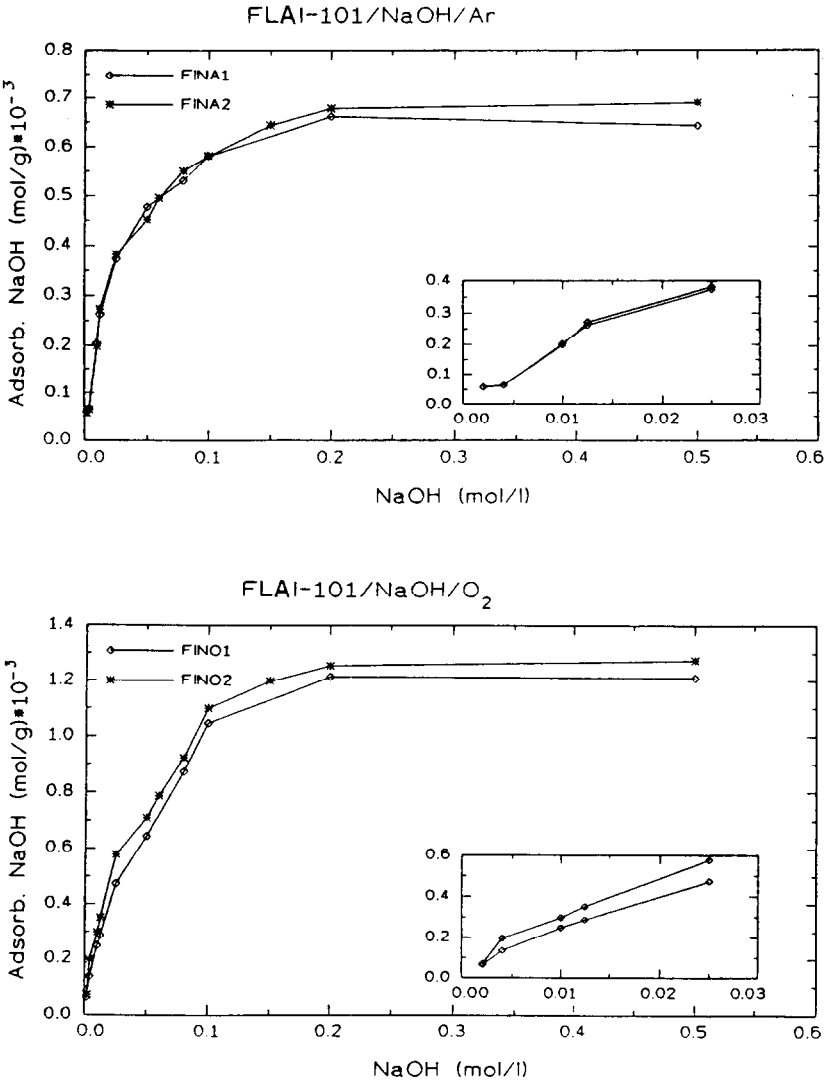


Fig. 1. Neutralisation isotherms for two carbon blacks (FLA 101 and FW 1) with NaOH under inert conditions and in oxygen atmosphere. The insets show the onsets of the isotherms indicating variable amounts of the highly reactive surface functional groups. The two data sets in each plot are from two different sample batches and indicate the reliability limit of the method.

at 300 K can also be seen in Fig. 1. The two carbons show different sensitivities to in situ oxidation, which is likely to convert weakly acidic groups into species more active in protolysis.

This analytical method can give access to the nature of the intermediate groups during carbon oxidation if the change of the p$K$ spectrum is followed as function of oxidation treatment. We would expect that at

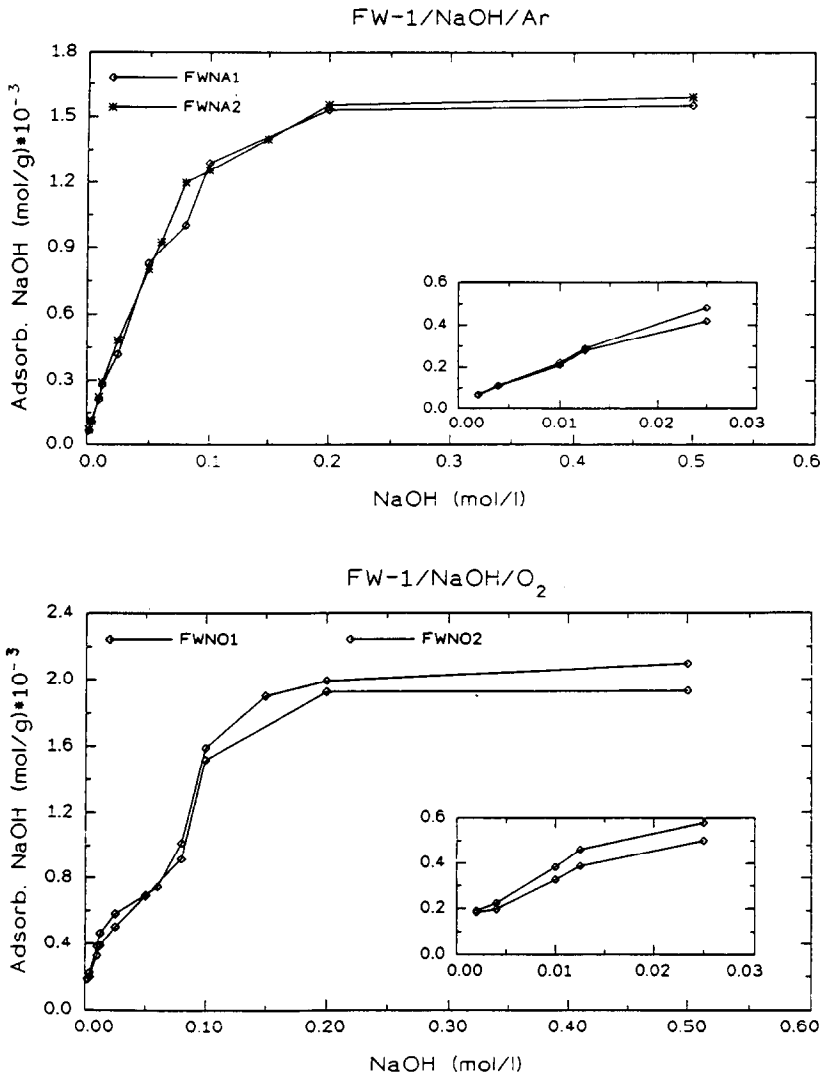


Fig. 1 (continued).

moderate reaction temperatures the number of functional groups increases, whereas at high temperatures the desorption of the final products $CO_2$ and CO during quench of the sample surface in an inert atmosphere will dominate and lead to a decreased abundance of functional groups. Exactly this behaviour was found. In Fig. 3 some quantitative data are displayed. The samples were cooled in the reaction gas atmosphere. Cooling in an inert atmosphere leads to surfaces essentially free of acidic hydroxyl groups after measurable burn-off.

In both carbons, acidic groups (p$K$ groups 1, 2) are more abundant than basic groups. The samples underwent low-temperature oxidation in their

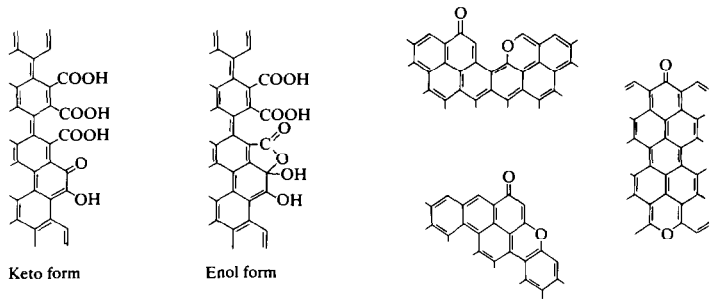


Fig. 2. Oxygen functional groups assignment of acidic and basic functional groups to possible chemical structures.

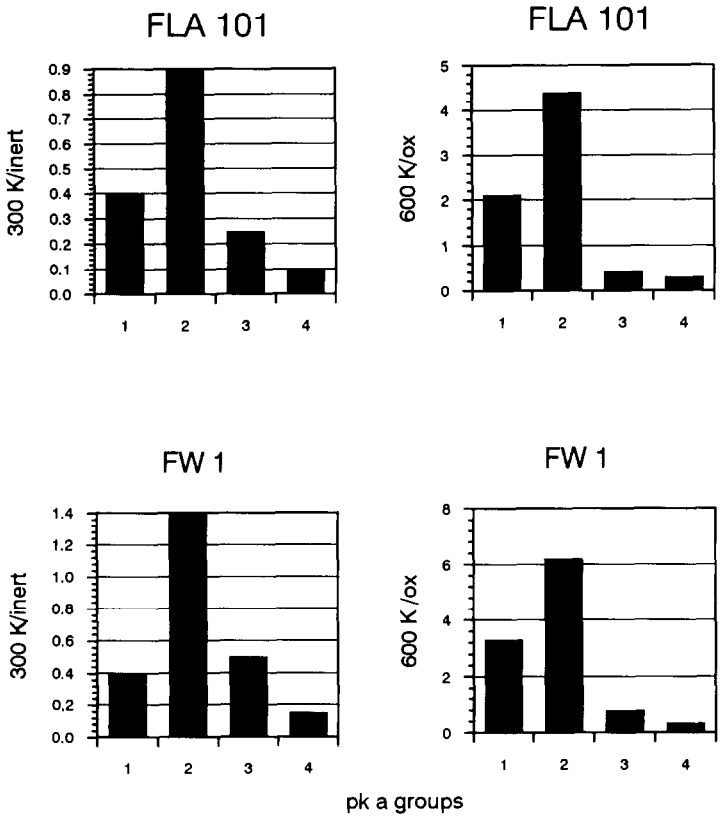


Fig. 3. Abundancies of various functional groups of carbon black in the as-received state (300 K, inert atmosphere storage) and after mild oxidation at 600 K. The differentiation in strongly and weakly acidic (species 1, 2) and basic (species 3, 4) groups was derived from crossover points in the linearised sorption isotherms, the abundances from extrapolations of the repective isotherm sections to saturation. The p$K$ values can be estimated from the neutralisation concentrations of about 0.1 mol $l^{-1}$ and 1.0 mol $l^{-1}$ for the strongly (species 1, 4) and weakly (species 2, 3) protolytic groups.

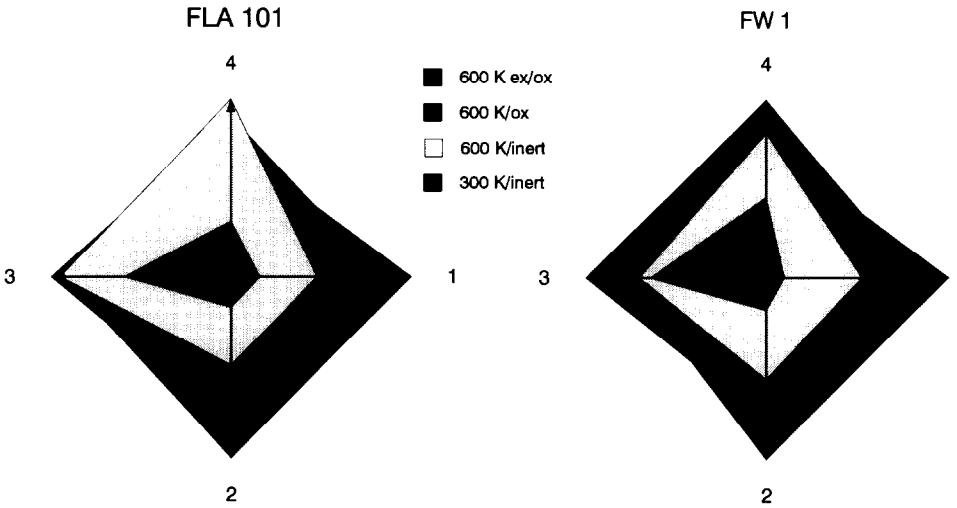


Fig. 4. Relative changes of the p$K$ distribution of two carbon blacks after different treatments. The four coordinates relate to the four types of species described quantitatively in Fig. 3.

history, as on-cleaned carbon literature reports [12, 13] an excess of the chemically more resistant basic groups. Oxidation increases the abundance of acidic groups drastically and also influences the relative concentrations of all groups, i.e. it modifies the p$K$ distribution. This modification is represented in Fig. 4 showing the p$K$ spectrum as four coordinates scaled in relative units. The four curves indicate the relative concentration of oxygen functional groups and the changes occuring after heat treatment in pure nitrogen, after oxidation in pure oxygen and after oxidation of extracted material. Inspection of Figs. 3 and 4 leads to the following conclusions:

(1) Different carbons react differently on heat treatment.

(2) The most abundant surface species generated during re-oxidation after significant burn-off are weakly acidic groups (coordinate 2).

(3) Acidic groups (coordinates 1, 2) increase in concentration without changing their relative abundance. The relative abundance of basic groups changes significantly.

(4) Extraction has an influence on the surface chemistry of both carbons; it leads in the acidic part of the distribution to an increase abundance. This points to an increase in reactive surface area. The clean-up is essentially effective on the outer surface of the carbon, as in porous FW1 the effect is not larger than in non-porous FLA 101.

(5) Heating in inert atmosphere produces an effect which must be caused by impurity oxygen (from adsorbed water and gas impurities; the nitrogen contained no oxygen detectable in a GC test) indicating the high reactivity of carbons at this temperature towards traces of oxidising agents.

(6) For further experiments we note that the study of oxygen

chemisorption requires removal of the hydroxyl groups first in order to access the reactive portion of the carbon surface and that any heating of a surface in even traces of oxygen will irreversibly change its structure as it will generate oxidation products.

(7) For the oxidation mechanism we learn that under the present relatively low temperatures acidic functional groups will form in larger concentrations than basic groups, which are initially present in excess; hence the formation of $CO_2$ should be the preferred elementary step. Under slow kinetic conditions each carbon atom is preferentially oxidised fully on the surface and not in the gas phase by homogeneous after-processes.

*Thermal desorption of functional groups*

Surface analytical studies of oxygen on carbon chemisorption require removal of the functional groups, a process which can be achieved using thermal desorption spectroscopy. Sufficiently high heating rates and small sample volumes ($3\,K\,s^{-1}$, 1.0 mg) lead to suppression of pore diffusion limitation and to well-resolved data as presented in Fig. 5. Only minor amounts of CO were desorbed in the temperature range analysed; acidic surface groups and the molecular water were removed in the cleaning procedure. Higher temperatures were avoided in order to minimise the irreversible surface oxidation indicated by the continuous rise of the $m/z$ 28 peak. Comparison of the $m/z$ 44 and $m/z$ 18 traces in Fig. 5 with the data in Fig. 3 allow one to conclude that water desorption below 600 K is due to

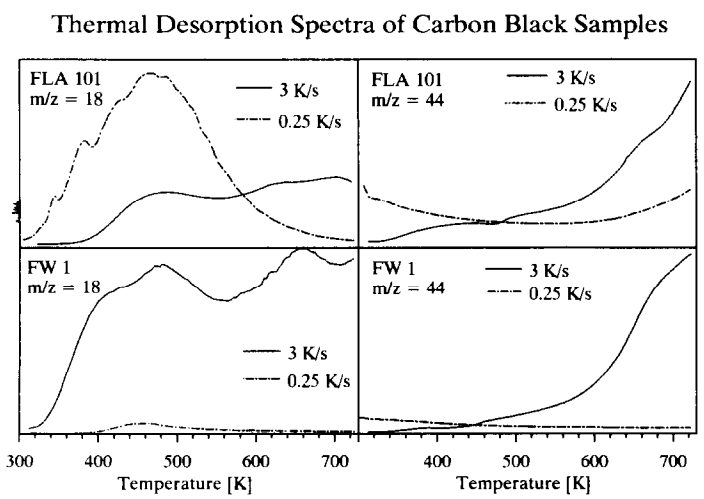


Fig. 5. Thermal desorption of water ($m/z$ 18) and $CO_2$ ($m/z$ 44) from two carbon blacks. The effects of the heating rate parameter on shape and intensity of the patterns are described in the text. All intensities are normalized to the BET surface area of the specimen.

desorption of molecular water bonded to highly acidic functional groups present in low abundance. The high-temperature water peaks coinciding with substantial $CO_2$ evolution indicate the removal of oxygen functional groups weakly active in protolysis or the reaction of commonly abundant C–H groups with basic oxygen functional groups. Both reactions involve the most abundant terminal groups on carbon [8, 12] which are, however, difficult to characterise chemically. The low-temperature water desorption from FW 1 points to a substantial amount of strongly acidic surface groups holding large amounts of molecular water. This is in agreement with the hydrolytic behaviour of the two blacks, a simple experiment in which FW 1 leads to a final pH of 3.2 and FLA 101 to essentially no reaction (pH 7.2).

The comparison between desorption experiments done in either the slow TPR regime or in the fast TDS range reveals the different limitations for the desorption kinetics. In FLA 101 slow heating leads to increased desorption due to chemical limitations; in FW 1 the pore diffusion/re-adsorption effects overcompensate for the chemical kinetic control leading to an inverse relation between fast and slow desorption yields.

An intensive search for other desorption products, e.g. aromatics or hydrocarbons was unsuccessful despite the sensitivity of the method for sub-monolayer amounts of adsorbates. It has to be concluded that those molecules which are removed by the toluene extraction do not desorb thermally below 700 K and may be oxidised during removal from the carbon surface at higher temperatures.

Desorption experiments, carried out in a less dynamic pumping environment in which the gas phase over the carbon is enriched during desorption with oxygenates, lead to significantly different desorption traces with no resolution above 500 K and increased amounts of $CO_2$ formation. The effect is in line with observations discussed with respect to Fig. 4 and underlines the high reactivity of the cleaned carbon surface against oxygenates.

*Chemisorption of Oxygen*

Precleaned carbon surfaces (heated twice to 780 K at 3 K $s^{-1}$) were exposed to molecular oxygen in order to study the chemisorption of the oxidant onto the carbon surface.

In low pressure–low temperature experiments ($10^{-6}$ mbar, 78–300 K) chemisorption of oxygen on active sites can be expected to take place without destroying the surface by oxidation. This is not, however, the case as concluded from extensive measurements with varying exposures. No sorption isotherms were obtained. Desorption temperatures and sorbed amounts indicated the creation of new sites with each desorption experiment even if the surface was only warmed to 300 K. A compromise between complete desorption and minimum irreversible surface oxidation

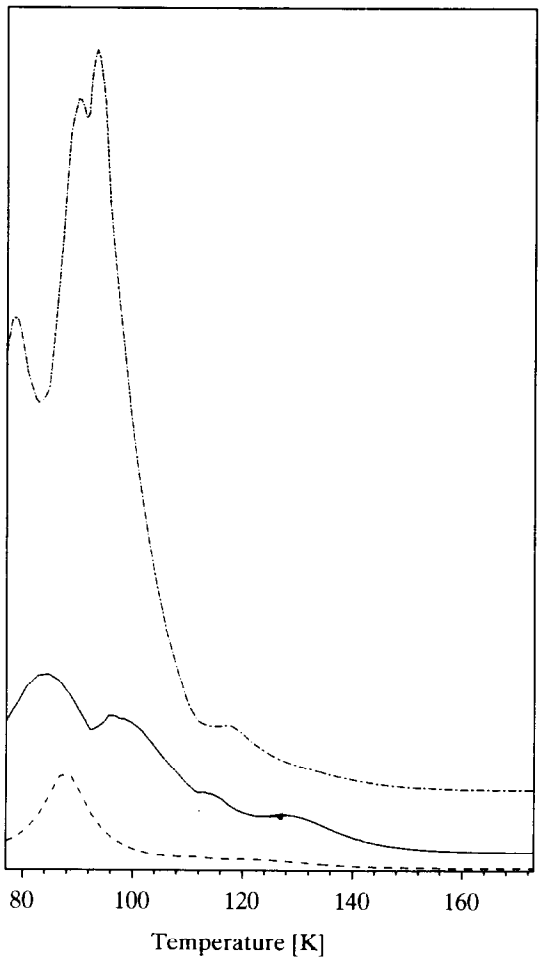


Fig. 6. Thermal desorption of chemisorbed molecular oxygen (signal intensity of $m/z$ 32 per unit weight) on pre-cleaned carbons: $m/z$ = 32, 100 Langmuir oxygen, heating rate 1 K $s^{-1}$. The intensities are normalized to the BET surface area of the specimen used. —, FLA 101; –·–·–, FW 1; – – –, HOPG.

was found with the parameters indicated in Fig. 6. In this series of experiment the substrate-specific differences are reproducibly analysed. It appears that each type of carbon has its characteristic fingerprint desorption pattern.

From surface science experiments with metal–oxgyen systems it is known that molecular oxygen with no bond dissociation desorbs below liquid nitrogen temperature and has not to be considered here. The peak around 95 K in Fig. 6 is attributed to a chemisorbed molecular oxygen species with some charge transferred from the substrate ("hyperoxo"). The alternative assignment of pore-diffusion limited desorption of physisorbed molecular oxygen is unlikely, at least with the HOPG surface. The features

above 100 K increase in intensity much less with increasing exposure than the main feature but exhibit sharp threshold exposures above 50 L. These observations and the fact that the features grow with increasing surface area of the sample indicate that these species are more strongly held at surface irregularities such as the prismatic edges of the stacks of $sp^2$ carbon layers constituting the macroscopic particles (see below).

The assignment of all structures in Fig. 6 to molecular charged species is only possible on the basis of photoemission experiments described elsewhere [4] which show the presence of oxygen molecules besides atomic oxygen (from the unremoved basic hydroxyl groups). The overall low desorption temperature is a further indication against an atomic oxygen species as this reactive species would not desorb as molecular oxgyen but rather as $CO_2$ or CO. Previous experiments with HOPG show that $CO_2$ is indeed desorbed above 150 K [14] where oxygen desorption is already terminated (see Fig. 6.) This result explains the creation of new sorption sites upon heating the carbon up to 300 K which was seen in sequential chemisorption experiments. It also shows that oxygen chemisorbed on immediate precursor sites for gasification is not observed in this experiment as no $CO/CO_2$ was produced below 150 K.

These data indicate that carbon oxidation may be a low-temperature reaction and carbon might be an air-sensitive material which is from practical experience, not the case. One reason for the ambient stability of carbon is not the insufficient reactivity towards oxygen but the activation barrier for the removal of site blockers such as hydroxyl groups present after exposure of carbon surfaces to moist air (see Fig. 5).

So far the oxygen chemisorption experiments have been carried out under unrealistically mild conditions. Using the high pressure attachment of the TDS system we exposed precleaned carbons to 10 mbar oxygen at 400 K for 5 min. Exposures at $10^{-6}$ mbar even for 24 h did not lead to any detectable oxygen desorption. Raising the pressure from $10^{-6}$ mbar to 10 mbar however caused considerable desorption features to appear which are displayed in Fig. 7. This threshold pressure effect is an indication for a different bonding state of the oxygen which is not accessible at low chemical potential. A peroxo [15] species with more negative charge on the oxygen molecule than in the bonding state seen in the low-temperature TDS experiments is a plausible chemical description of this bonding state desorbing from all surfaces at 420 K. The width of the peak indicates a distribution of chemisorption sites for this species.

The peak area does not scale with the BET surface area of the carbon material as the number of active sites for oxygen chemisorption is not equal for different types of carbon. Kinetic artifacts are unlikely at the low heating rate chosen and in the absence of any dependence of the peak area on the exposure time.

The additional low-temperature species present in all spectra of Fig. 7

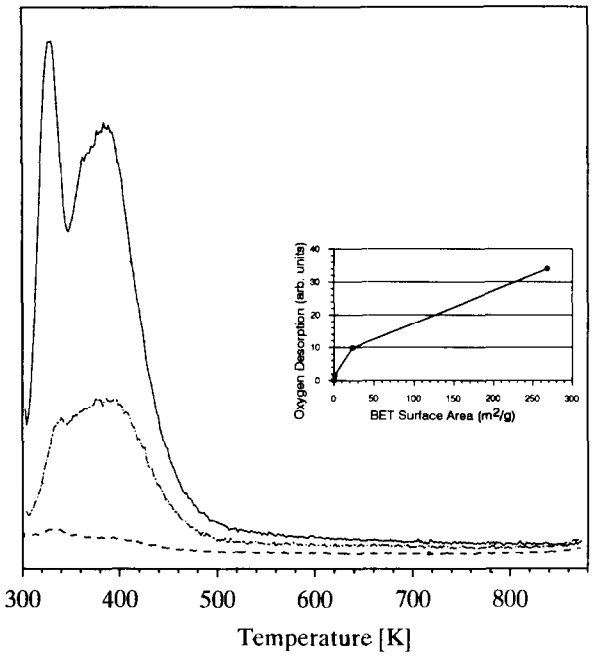


Fig. 7. Thermal desorption of strongly held molecular oxygen chemisorbed at 400 K in 10 mbar oxygen: $m/z = 32$, heating rate 0.25 K $s^{-1}$ signal intensity per unit weight. The inset shows that the active surface area (area under the desorption peak) does not correlate linearly with the geometric surface area (BET) for the three different carbon surfaces. —, FW 1; –·–·–, FLA 101; – – –, graphite.

desorb below the exposure temperature. The size of the peak scales with the surface area of the specimen which excludes a sample holder artifact as explanation. This oxygen was adsorbed during cooling of the sample in oxygen. Exposures at lower temperatures drastically reduced the intensity of this feature. All this indicates that the presence of the high-temperature species enhances the abundance of the low-temperature species on the surface which may be the precursor of the main high-temperature oxygen. Chemisorption of oxygen on carbon may be autocatalysed in such a way that more stable forms of carbon–oxygen bonds enhance the surface abundance of weakly held species and so increase the rate of formation of the more strongly held form.

Desorption experiments at higher temperatures have been described in the literature [2]. They indicate the co-existence of several molecular and atomic oxygen species with intermediate hydroxyl species and illustrate a whole chain of processes necessary for carbon oxidation.

In order to understand the initial steps in such a chain of reactions, the dissociation of oxygen on carbon via negatively charged molecular precursors, we studied the surface electronic structure of carbons. The most relevant problem is the determination of the hybridisation state as only $sp^2$

carbon centres may transfer electrons to oxygen and so help the dissociation at low temperatures by occupation of anti-bonding molecular orbitals.

*Electronic structure of the reacting surface*

Conventional photoemission, such as XPS or UPS, is fairly insensitive for reliably detecting the differences in surface electronic structure of different carbon materials [11, 16]. X-ray absorption spectroscopy (XAS) on the carbon *K* edge was, however, found to be a suitable tool. The principal application to carbons was described in a previous paper [11]. In Fig. 8 the main features of the method are demonstrated on a sample of HOPG. The figure shows a series of polarisation-dependent spectra and the assignment of all peaks of the antibonding conduction bands to the calculated band structure of graphite. Features G and A are pure $\sigma^*$ and $\pi^*$ state derived resonances. The observation of their polarisation dependencies allows the determination of the degree of surface ordering and of the ratio between $\sigma^*$ and $\pi^*$ surface states: measurements at high angles (as defined in Fig. 8) are $\pi^*$-state sensitive; experiments at low angles detect $\sigma^*$ states. The analysis requires well-defined surfaces which are not available with powdered carbons. Here only relative changes between features as a function of surface treatments can be analysed. Additional information is obtained in the partial yield detection mode in which a variable retarding field allows discrimination of surface-sensitive Auger electrons from bulk-sensitive secondary electrons. In this way a non-destructive qualitative depth profiling can be carried out independently of sample crystallinity.

Analysis of the polarisation dependence of spectra from HOPG surfaces after cleavage (well-ordered), after oxidation in air (optically rough) and after Ar ion sputtering (optically smooth) showed [11] that oxidation introduces only few additional surface defects and little integral changes in the surface electronic structure, i.e. is only a local phenomenon with no long-range consequences, whereas sputtering destroys the whole surface orientation and considerably reduces the number of $sp^2$ carbon atoms in the surface. Verification of the absence of pronounced cooperative electronic effects of oxidation is a prerequisite for topotactic reaction control.

The problem of identification of the effect of solvent extraction was analysed with the XAS method. Extraction modifies the surface reactivity (see Fig. 4) but TDS gave no indication of desorbing molecules. A monolayer of polycyclic aromatic molecules (formed during genesis of the carbon in sooting flames) strongly chemisorbed to the surface of the hydrogen-free carbon may be compatible with the missing TDS observation. In this case the surface should be more "aromatic" in character as the bulk carbon contains a large number of crystallographic defects and a small degree of graphitisation [4]. Figure 9 shows XAS spectra of FLA 101

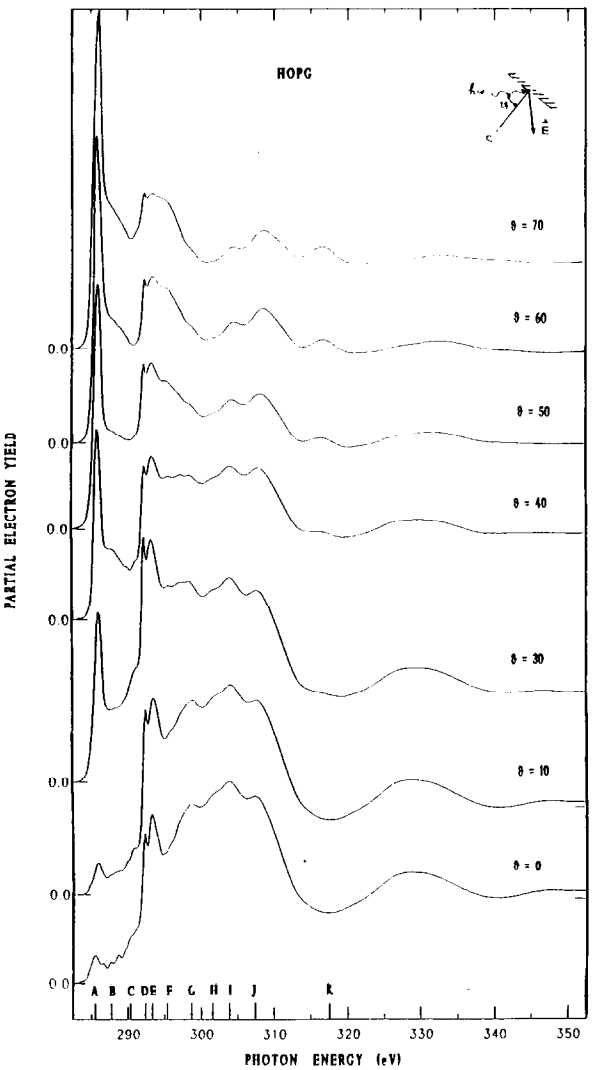


Fig. 8. XAS spectra for HOPG. The polarisation dependence shown allows the unambigous assignment of the peaks to $\sigma$ (low angles) and $\pi$ (high angles) unoccupied electronic states. The features A–K can be assigned to peaks in the theoretical density of states (see text).

before and after extraction (transferred under strict exclusion of air) in a detection mode of high $\pi^*$ electron specificity and of high surface sensitivity. It can be seen very clearly that the extracted carbon is richer in $\sigma^*$ states at the surface and that the total electronic structure of the extracted carbon is different from that of the aromatic overlayer (distance between onset of $\sigma^*$ region at 294 eV and first $\pi^*$ resonance), which in its energetic positions of the resonances is indistinguishable from graphite. XPS data showed that the spectroscopic initial C1s state is unchanged in

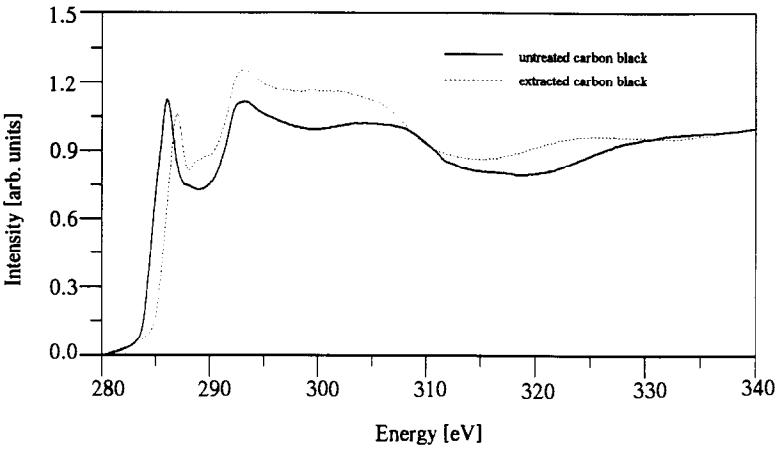


Fig. 9. Carbon *K* edge XAS data of FLA 101 before and after solvent extraction intended to remove aromatic molecules from the carbon surface (partial yield 100 V, 60 degrees).

the two samples. This illustrates the insensitivity of the XPS method to the small difference in electronic structure between aromatic molecules and defective $sp^2$ carbon.

The XAS experiment, which gives similar results for other carbon blacks, is strong supporting evidence for the presence of a firmly held surface layer of aromatic molecules which can be (at least in part) removed by the action of a solvent. The existence of such a temperature-stable layer of molecules on the solid interface has significant implications for the surface chemistry and hence for the practical application of carbon blacks.

The XAS data further show that well-ordered graphite is only in part a suitable model for other $sp^2$-type carbon materials such as the carbon blacks used here or soot or even coal. The electronic deviations from a metallic delocalised $\pi$ electron system centred at each surface atom are significant as follows from the comparison (Figs. 7, 8) of XAS spectra of these materials. The significance of this finding in the present context is that the possibility to transfer electrons to chemisorbed oxygen is not given on each surface site. The distribution of sites may be associated with basal and prismatic faces because in XAS of powered carbons a significant fraction of the total surface will not be oriented with the basal planes of the basic structural units perpendicular to the incoming photon beam. Angular dependence measurements indeed show a texture of about 5% relative to the orientational ordering of HOPG. If this analysis were correct, no change of the degree of hybridisation should be detected during burn-off as the basal-to-prismatic edge ratio will not change drastically during oxidation of at least the first 50 wt% of the sample.

The basal planes of the material contribute, however, overproportionally to the surface-sensitive XAS data due to the platelet anisotropy of the graphitic basic structural units. For the carbon oxidation mechanism it

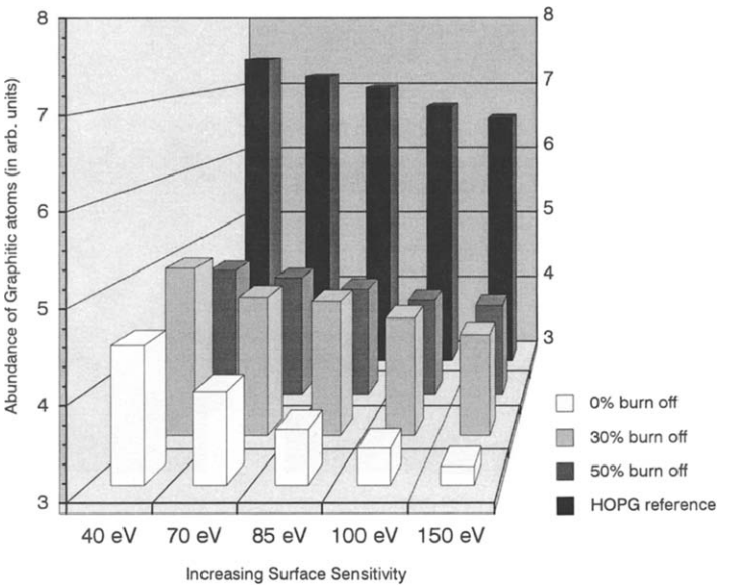


Fig. 10. Analysis of the graphitic character of FLA 101 carbon black after various treatments by partial yield XAS. The voltages given are the retarding potentials which, with increasing values, reduce the contribution of non-surface sensitive secondary electrons to the detected signal.

would be important to know if the surface is enriched in defects relative to the bulk and whether the abundance of $sp^2$ carbon atoms increases during oxidation as a consequence of the prefered defect etching. In this case it would be concievable that as a function of burn-off the factor controlling the overall kinetics will change from activation of molecular oxygen (too few electron-rich sites) to the gasification regime (too few defective sites for oxygen attack).

Partial yield XAS of partly oxidised carbon blacks were analysed for the abundance of $sp^2$ centres by integrating the area under the first $\pi^*$ resonance of spectra normalised to the height of the edge jump. The results for HOPG as reference and for FLA 101 can be seen in Fig. 10. The carbon black contains about 40% of the $sp^2$ carbon atoms present in freshly UHV-cleaved HOPG. In all carbons the surfaces are more defective than the bulk regions. The absolute information depth of the method can only be estimated to be about 10 monolayers for the 40 eV data and about 3 monolayers for the 150 eV data. Burning the carbon preferentially removes defective centres [5, 6, 8, 17], significantly more at the surface than in the bulk. Extensive burn-off further improves the surface graphitic character but introduces new defects in the bulk. This finding is in full agreement with a topotactic reaction progress not only in flat HOPG but also in the x-ray nanocrystalline carbon material. Edge recession and excavation by pit erosion are the two expected mechanisms of carbon loss which are compatible with the above results.

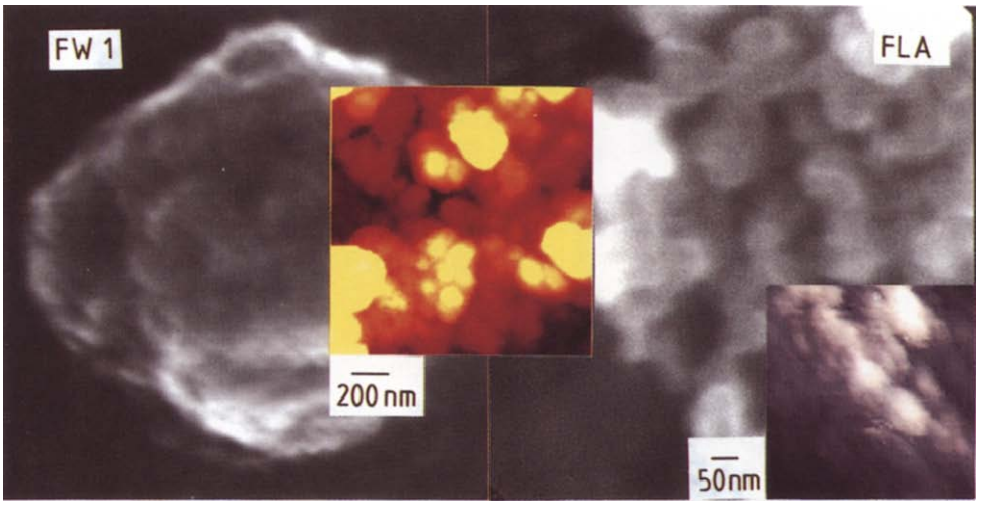


Fig. 11. Comparison of SEM (large images) and STM images of the two carbon blacks in the as-received states. Uncoated samples were investigated in a Jeol JSM 35 at 15 kV for SEM and studied in air with a Pt–Ir tip in the STM (400 mV bias, 2.0 nA current, constant height mode).

*Microstructure of the carbon surface*

Microstructural investigations are required to vaildate the spectroscopic indications for the oxidation mechanism. A combination of spectroscopy yielding quantitative integral information, with high resolution microscopy, allowing local resolution of the geometric situation of a reacted surface, is a suitable approach to back up a kinetic analysis of the reaction.

Figure 11 shows survey images of the two black materials with SEM and STM. The chosen magnification scale is in the overlap region of the two methods, so allowing direct comparison. The FLA sample consists of flat aggregates of basic structural units. These flake-like units form large aggregates called "structure" in the carbon black literature. The STM image reveals that in SEM flat objects still exhibit significant internal structure arising from the arrangement of the basic structural units [2]. The FW 1 material is of quite different secondary structure, being much more isotropic. The spherical particle in the SEM. image is composed of aggregates of smaller spherical particles seen in the STM. The different sources of carbon formation lead thus to different agglomeration schemes of the basic structural units which are rather similar in their dimensions as revealed by TEM, STM and X-ray scattering. The different aggregation modes can yield different basal-to-prismatic surface area ratios and so significantly affect the oxidation kinetics.

High resolution imaging of oxidised carbon surfaces in the STM is only possible with graphite (either in particulate form or as HOPG), but not with carbon blacks. This is a consequence of the high surface area defect

density leading to many chemisorbed adatoms (about 10 hydroxyl groups in a typical image area such as in Fig. 12, estimated from the acid–base chemisorption data) and to overall poor electrical surface conductivity. The number of surface atoms having no contact with the 2D metallic electronic systems is on graphite, even after severe oxidation, only small and the insulating effect is locally limited. Such practical experiences from the STM work are in agreement with the XAS data outlined above.

Starting on HOPG we first discuss the undisturbed atomically resolved image of graphite. In Fig. 12 two typical images are shown. The hexagonal array represents exactly the expected structure with geometric parameters compatible with the Bernal graphite structure. This image is very rate on graphite but can be obtained in the vicinity of defect lines in thin and carefully horizontally cleaved HOPG specimens. The common image used as calibration standard in the STM is the triangular pattern [18] also displayed in Fig. 12. It represents an interference pattern of two graphene layers. The exact mechanism is still the focus of controversy in the literature and several explanations [19, 20] have been proposed all of which may operate in a single STM data acquisition.

It is pointed out that the present images were obtained in air at 300 K, conditions under which the surface is clearly covered with water, oxygen and other adsorbates (see the TDS part of this paper and the literature [21]). The adatoms are either electronically transparent [22] or are removed by the action of the STM tip and the concomitant electric fields. The density of the firmly bonded hydroxyl groups on graphite surfaces is so low that they may all be located on prismatic edges where STM is difficult to perform. For oxidation studies it appears that chemisorbed molecular or even atomic oxygen as detected in the TDS experiments cannot be imaged by STM in air under ambient conditions.

The topographic effects of topotactic oxidation with preferred reactivity at defects can, however, be imaged conveniently by STM. Such studies were performed much earlier by conventional microscopy but the limited resolution required either substantial oxidation [8, 26] with no chance to see the beginning of the reaction or complicated specimen preparation procedures [5].

In Fig. 13 the typical surface modifications on HOPG after oxdiation in air at 900 K are displayed. The 400 nm wide etch pit is one monolayer deep (Fig. 13b) and results from a single point defect in only the top graphene layer. It is an example of topotactic reaction control as only prismatic faces can gasify and hence no attack of deeper graphene layers occurs. It further shows that no defects are introduced in deeper lying graphene layers, indicating that the mechanism does not involve radical atomic species as long-living intermediates which could migrate and unselectively attack [23] the graphene $\pi$ electron system. The deep structure in Fig. 13 arises as an etch pattern of a cooperative three-dimensional crystal defect such as a

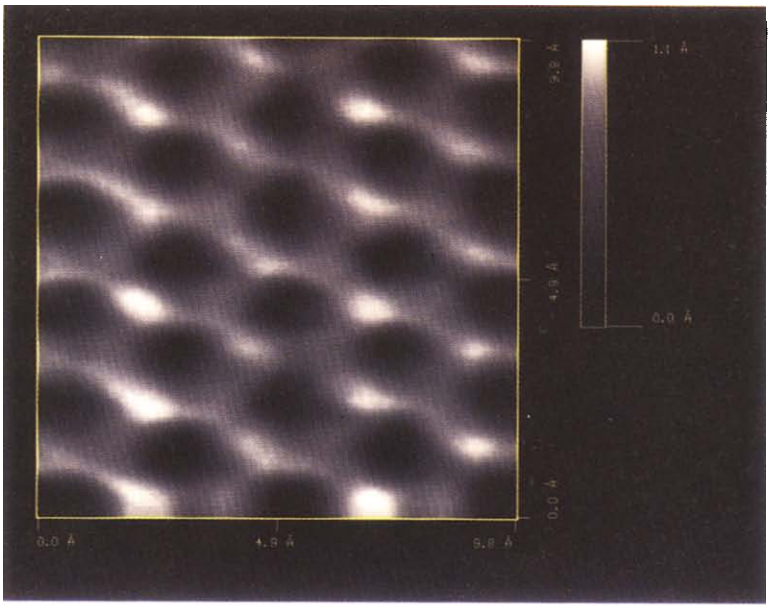


(a)

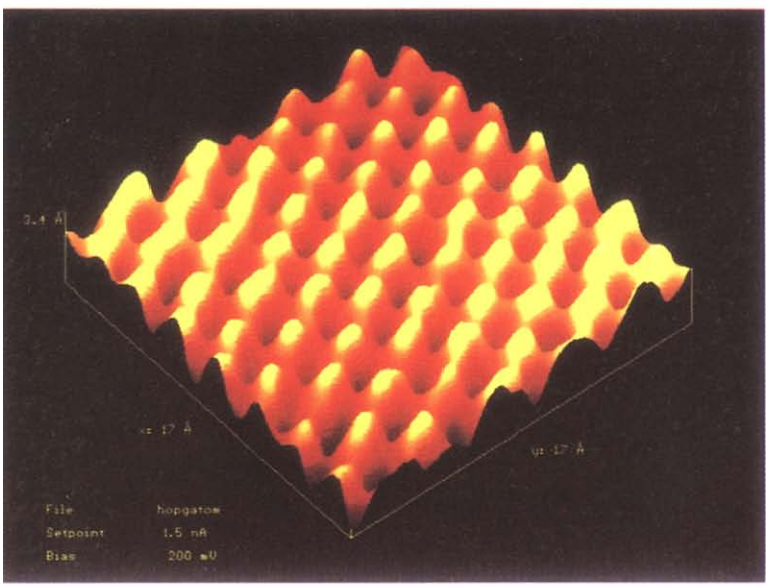


(b)

Fig. 12. Atomic resolution STM from HOPG (scan areas 1.7 nm × 1.7 nm and 0.98 nm × 0.98 nm).

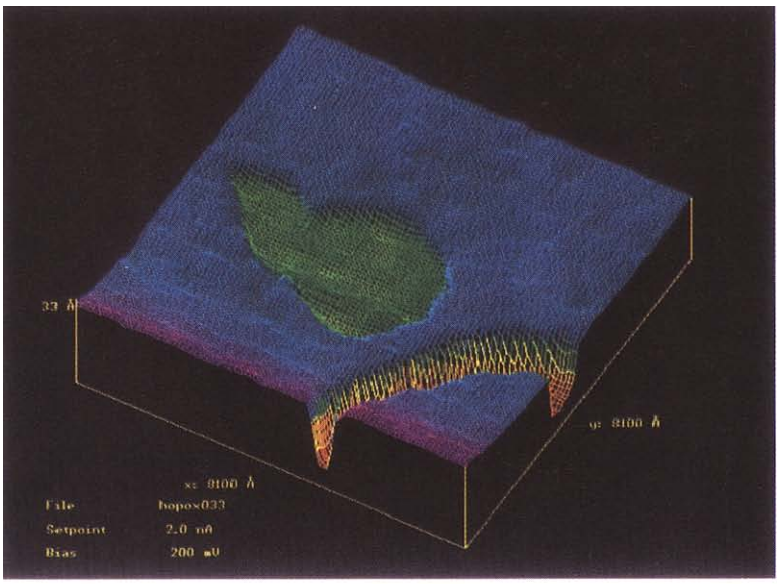


(a)

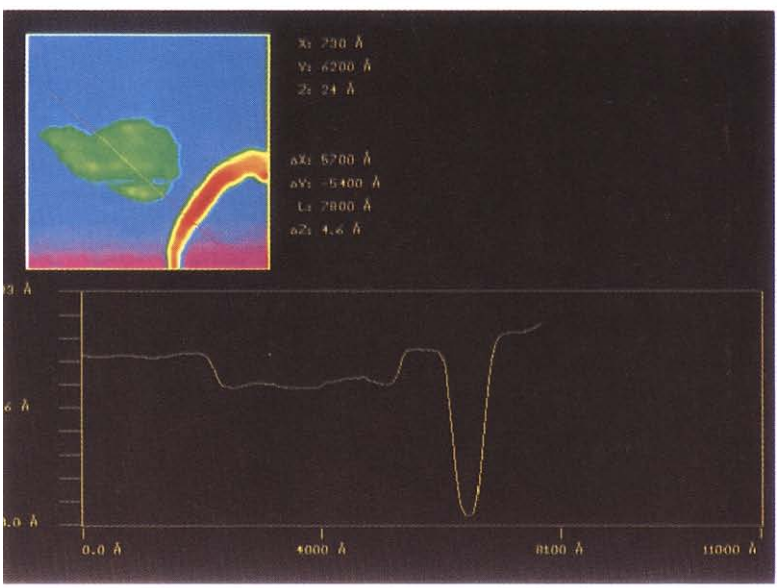


(b)

Fig. 13. A typical surface of oxidised HOPG (air, 900 K), (scan area 810 nm × 810 nm).

grain boundary. Its true depth cannot be measured by STM as the tip properties may well limit the penetration into the 20 nm wide entrance of the slit. Such a structure does not generate additional reactive sites as the prismatic face surface area remains constant during reaction. Consequently, we see two two-dimensional reaction fronts widening the slit. The 2D etch pit on the basal plane does, however, create new reactive sites at its growing perimeter and hence influences the local reaction kinetics with ongoing burn-off.

Particulate graphite such as the RFL sample provides the opportunity to image crystal edges and prismatic faces [10]. In Fig. 14 images from a stepped crystal edge and at high resolution from one terrace of that area again indicate the controlled reaction with parallel edge recession and the integrity of the graphite electronic structure on the basal planes next to the reaction zones. The noise in the atomically resolved image indicates the presence of some adsorbates on either the surface or the tip interfering with the tunnelling process. Tip worsening is common in imaging such rough structures; in the present samples occasional crashes between sample and surface could not be avoided. In the survey image (Fig. 14a) the following features can be identified: (1) The defect structure of the individual graphene layer packages forming the steps and terraces are preferentially etch-decorated and generate irregular trenches perpendicular to the main reaction direction. (2) The step edges are terminated in a zig-zag fashion which is not a scan artifact from the STM. (3) The local electronic structure at the edges is different from that of the terraces giving rise to the apparent bending of the edge area with a height difference of about 0.1 nm. (4) The velocity of edge recession is constant over comparatively large areas as all edges remain straight and parallel to each other. Such highly coordinated reaction behaviour is characteristic for samples with substantial burn-off (30%–50%); in the initial stages irregular removal of graphene layer packages folded over crystal edges (see images in the literature [27]) occurs.

Reaction edges created from point defects on basal planes often exhibit highly irregular perimeters and do not represent the crystal symmetry of the bulk material. An example of a three monolayer high reaction front on the basal plane of RFL graphite is shown in Fig. 15. At low magnification in the SEM such reaction fronts appears straight but the STM clearly resolves localy varying reaction velocities leading to the irregular microshape. The enhanced contours at the edges (see "overshootings" in the cross section profile of Figs. 15b and 17b) arise from a tip artifact in combination with a locally disturbed electronic structure (work function change due to $sp^3$ atoms and heteroatoms) as was shown by observing the change of the contours as function of scan parameter variation (direction, speed, tip-to-surface distance, operation mode and gap voltage).

The bent trench in the lower part of Fig. 15 is one monolayer deep and 30 nm wide. It is attributed to the trace of a catalyst particle of probably a

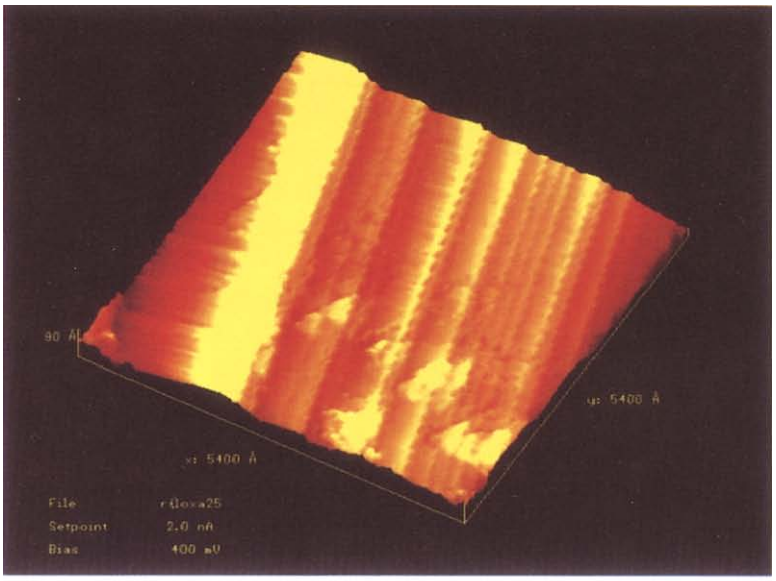


(a)

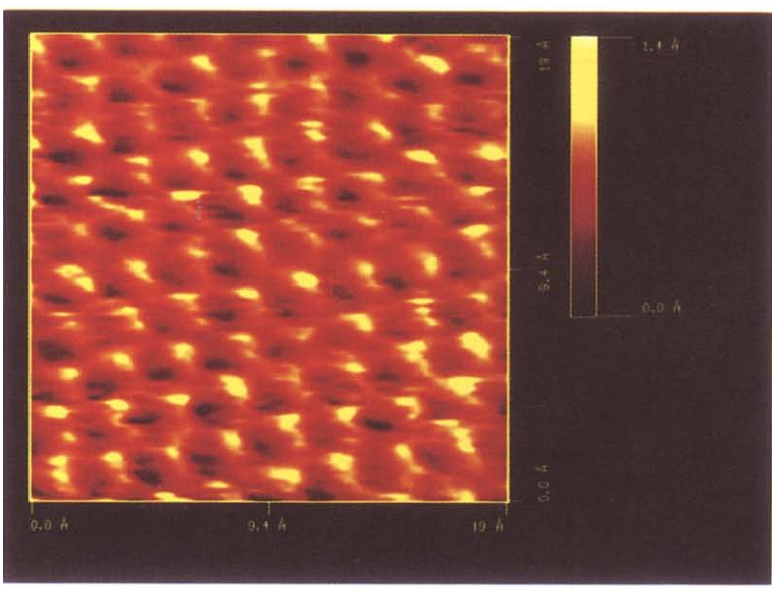


(b)

Fig. 14. STM of partly oxidised RFL particulate graphite (air, 900 K), (scan areas: (a) 540 nm × 540 nm, and (b) 1.9 nm × 1.9 nm).

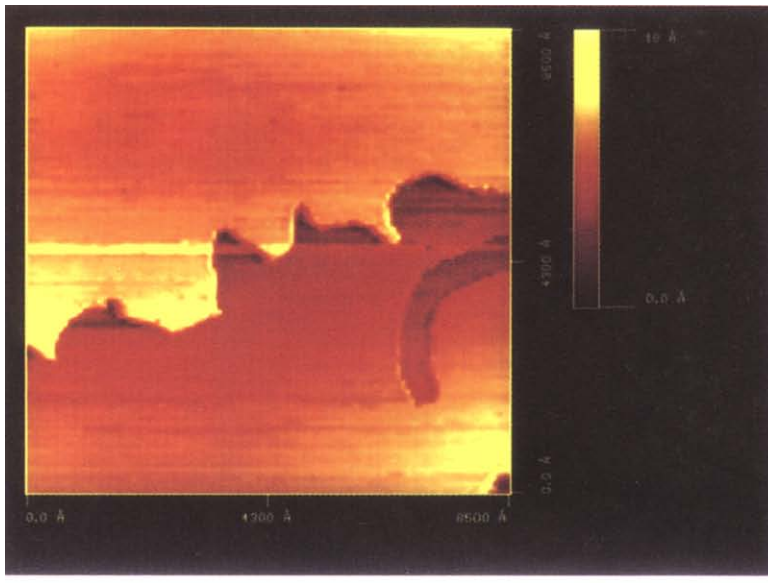


(a)

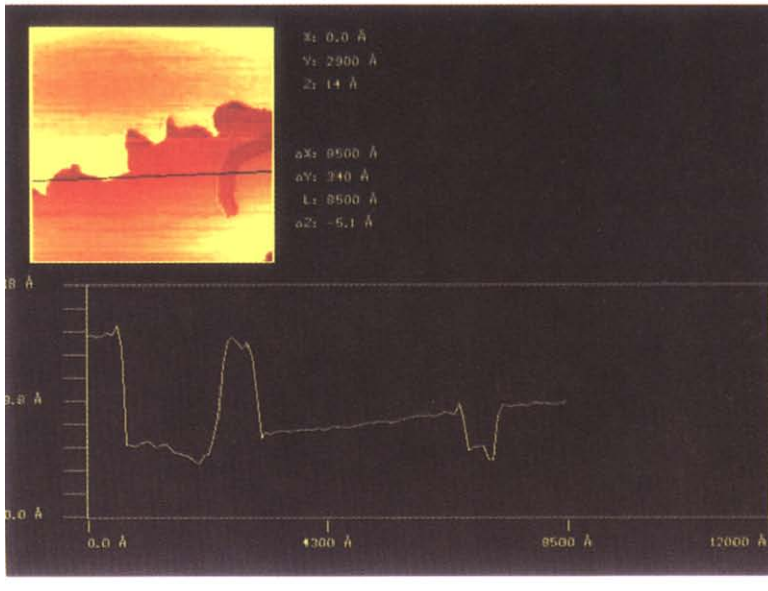


(b)

Fig. 15. Reaction fronts on the basal planes of RFL particulate graphite after oxidation in air (scan area 850 nm × 850 nm).

transition metal; it is well known [24, 25] that these particles scan rapidly over the surface in an irregular fashion leaving behind shallow ditches as seen in the figure.

In HOPG the defect density within a single graphene layer can be high leading to a totally irregular recession of the top layer. In Fig. 16 such a situation is displayed in which no correlation exists between the reaction edges of the top layer and the second layer (etch pits in the lower left corner of the image). Such reaction behaviour cannot be accounted for by observing or extrapolating average edge recessions from the crystal edges. The continuous topotactic reaction (top edge recession and prism face reaction) is superimposed with a statistical second reaction channel depending on the defect distribution in each graphene layer. The image also illustrates that the contribution of that second channel to the local total reaction rate can be substantial, as the external prism faces representing the primary reaction fronts of the top graphene layers are outside the image area of Fig. 15 and so no reaction should arise from the area imaged in Fig. 15. The noise in the image is a clear indication of the presence of adatoms, as flash heating of the surface in inert atmosphere under desorption of $CO_2$ removes the irregularities in the scan profiles.

If the oxidation starts from a single point defect in the basal surface the concept of toptactic reaction control predicts the formation of hexagonal etch pits with (100) and (110) prismatic faces serving as edges. In literature studies such situations after prolonged reaction producing macroscopic pits were described as being frequent [26]. In cases of loop shaped aggretated surface defects, circular etch pits can arise which have in their early states also been imaged before using TEM and a gold decoration technique [5]. Surface defects may propagate through deeper graphene layers with their orientation at an arbitrary angle to the graphite *c* axis. Such a situation in RFL graphite is shown in Fig. 17. The point defect initiating the second-layer etch pit was not located exactly under the top point defect. The profile as well as the image show significant irregularities at the edges of the pits preventing the reliable measurement of the step height at the location chosen for the profile. These irregularities are caused by the chemisorbed oxygen functional groups eliminating the electrical conductivity at the edge. These STM artifacts are direct proof of the decoration of prismatic edges by heteroatoms. The apparent gaps in the scan profiles penetrating deeper into the material are also artifacts caused by the irregular electronic structure at the reaction front and bear no topographic relevance.

In Fig. 18 a surface defect on the basal plane of partly oxidised HOPG acting as possible reaction site is imaged. Termination of a dislocation loop led to a sequence of monolayer terraces. The overall contours of regular crystallographic directions decorated by the step edges can be seen. The inset displays the two-dimensional Fourier transform of the image

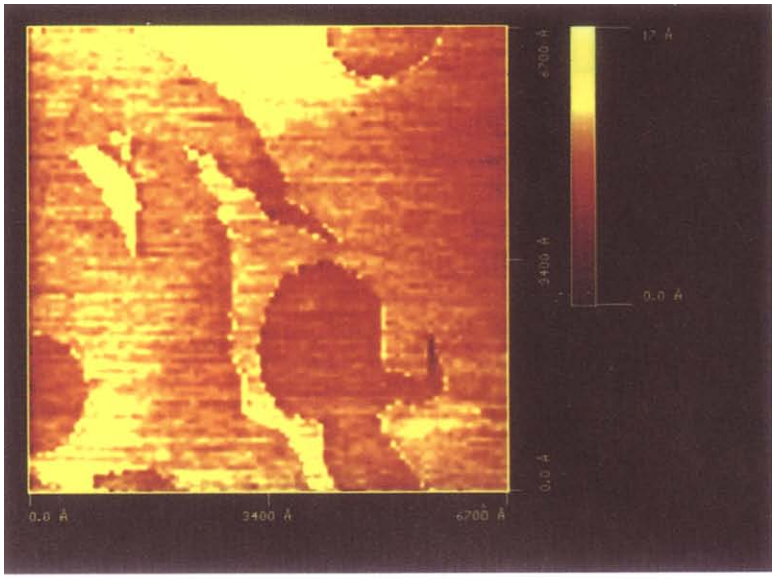


(a)

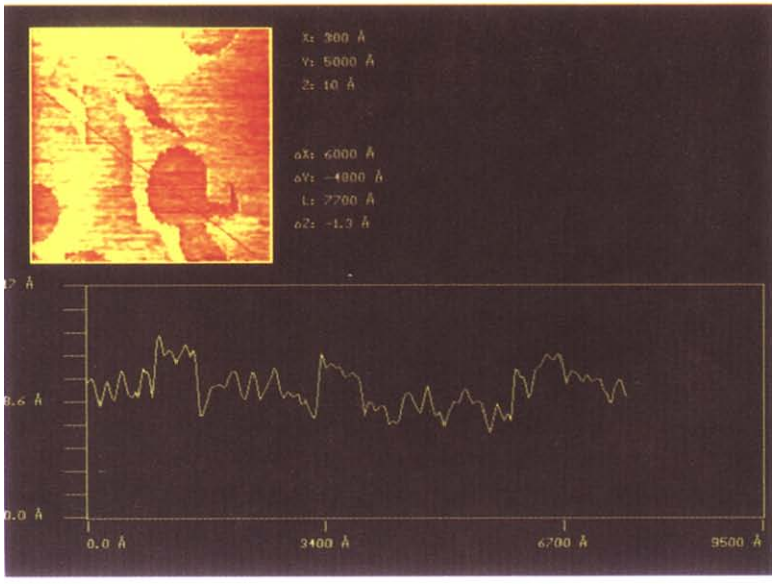


(b)

Fig. 16. A basal plane view of partly oxidised HOPG (different sample from Fig. 13, but same conditions) (scan area 670 nm × 670 nm).

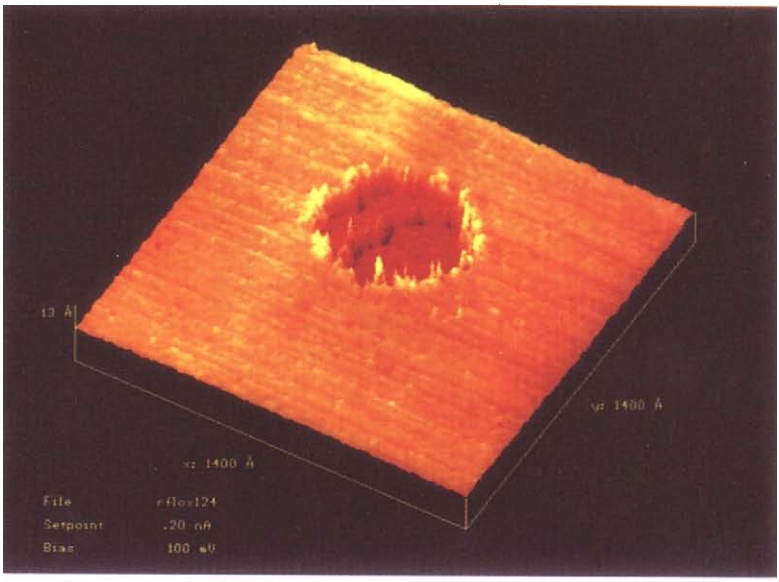


(a)

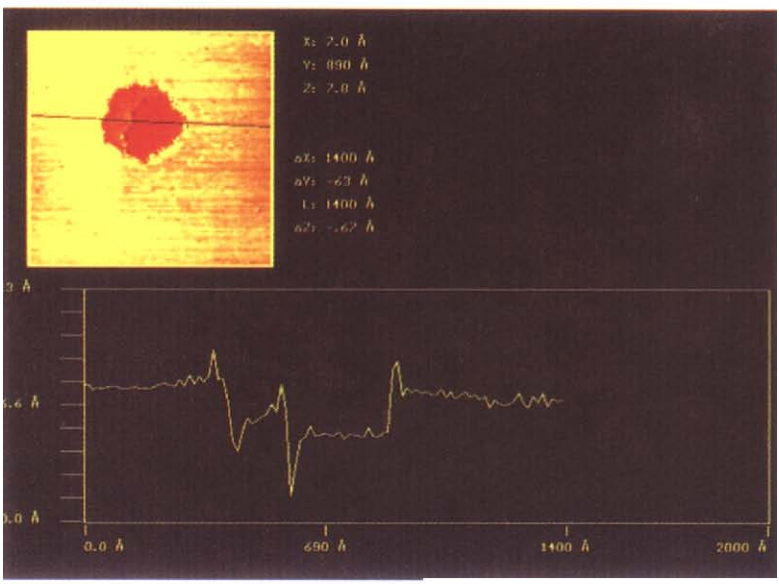


(b)

Fig. 17. Etch pits from isolated point defects on RFL particulare graphite. (scan area 140 nm × 140 nm).

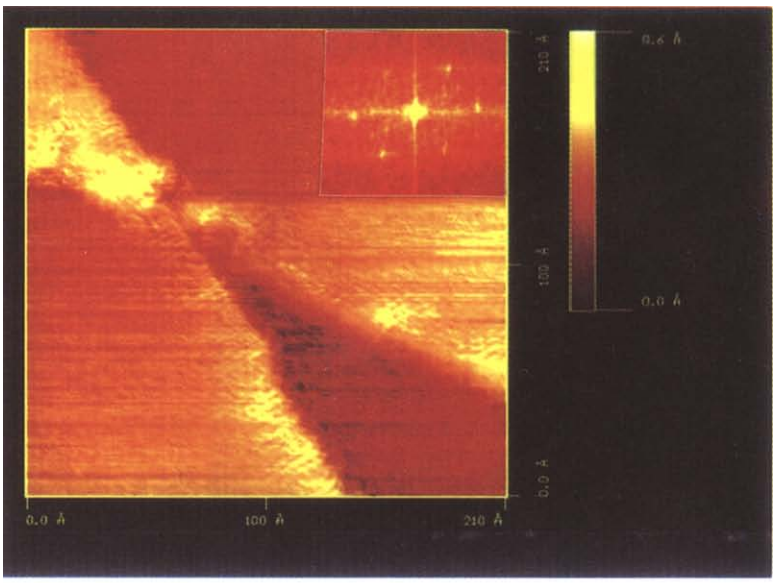


(a)

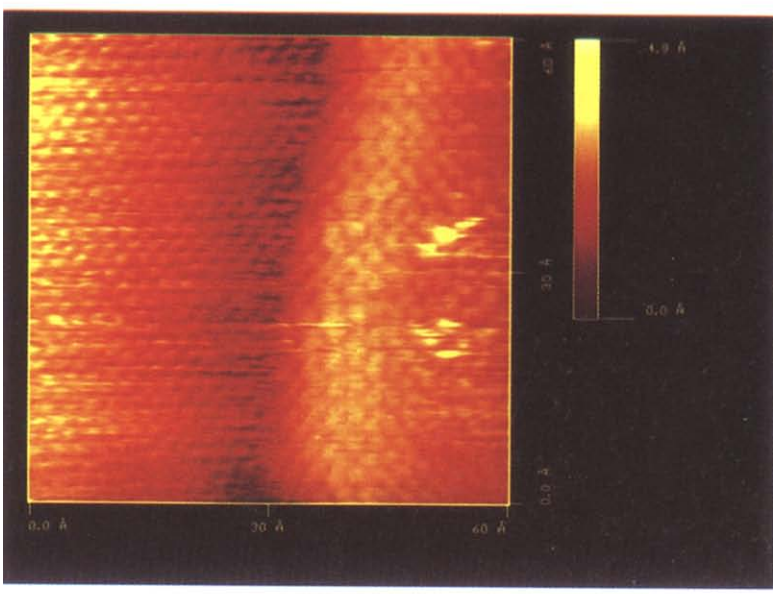


(b)

Fig. 18. High resolution STM images of a reaction front on HOPG oxidised at 900 K in oxygen (scan areas: (a) 21 nm × 21 nm, and (b) 6 nm × 6 nm; heights: (a) 0.86 nm, and (b) 0.49 nm for the full colour scales). The inset on the main image is the 2-dimensional Fourier transform showing the expected diagonal symmetry of the atom arrangement in the graphite (001) basal plane.

indicating that the hexagonal graphite structure is present in the noisy image. Figure 18b shows an enlarged section of a monoatomic step. The irregularity in the atomic structure near the edge can be seen clearly. The arrangement of the individual carbon atoms is the same trigonal superstructure as seen in Fig. 12 with the two terraces being rotated by 5°. The apparent arrangement of hexagonal close packed atoms at the very edge is compatible with a terminating single graphene layer. At present it cannot be decided if these images, which we obtain frequently, indicate a reconstruction of the edge by the breaking of C–C bonds or if it is an imaging artifact [22] arising from the modified electronic structure which produces a superposition of the underlying terrace atoms with the edge atoms. The colour height code further illustrates that the edge is not a parallel step but appears as wedge-shaped with an enlarged step height reaching about 4 atom rows deep into the terrace. This is not a tip artifact as it does not depend on scan direction or on tip change. A topographic interpretation is, however, not possible without knowing the local electronic structure at the step which will be accessible in the future [28].

## CONCLUSIONS

Chemical analysis revealed the complexity of surface hydroxyl groups and the changes in the p$K$ spectrum upon thermal treatment. This is taken as indication that the average local geometry of defect sites, to which the hydroxyl groups are coordinated, do change during thermal treatment. In these early stages of combustion the topotactic control is thus expected not to be constant and no meaningful kinetic law will be derived.

The overall electronic surface structure was investigated by XAS, showing for carbon blacks a change in the degree of surface graphitisation as function of oxidative treatment. The expected decrease in graphitic ordering due to defect etching is, over significant parts of the total burn-off, overcompensated by the preferential loss of defect sites allowing the degree of graphitisation to pass a maximum which will be different in each type of carbon.

At moderate temperature thermal treatment removes the acidic surface groups. The remaining surface defects can act as efficient centres for oxygen chemisorption. A weakly held anionic molecular species is chemisorbed at low temperatues and low exposures. Its conversion into a second more strongly held molecular species desorbing at 420 K requires significant activation which finds its expression in pressure and temperature thresholds.

A variety of local geometric structures on carbon surfaces were imaged by STM. The irregularities at edges in either the electronic or in the geometric atom arrangement were clearly established. A simple model of a regular terminating graphene layer seems not to adequately describe the

situation at the reaction fronts. The generation of new reaction fronts via defect etching often does not lead to regular etch patterns but to irregular contours documenting the involvement of several defect types and locations in the formation of the new reaction fronts. On long reaction fronts starting from steps in the crystal surface the effect of embedded point defects on the microshape of the reaction front has been illustrated. This is no violation of a two-dimensional topotactic reaction control.

All these findings are ingredients in a description of the overall complex oxidation reaction of carbon. Much more work is now required to quantify the phenomena and to investigate the influence of the average carbon structure on these parameters in order to find experimental foundations for a numerical kinetic model allowing description of this "chemically very simple" reaction.

## ACKNOWLEDGEMENTS

The XAS activity has been carried out in joint collaboration with the group of A.M. Bradshaw, Berlin. We acknowledge the help of Th. Schedel-Niedrig, M. Keil, H. Werner and D. Herein with the synchrotron experiments. Financial support came from Du Pont, the Fonds der Chemischen Industrie and the Hermann Willkom Foundation.

## REFERENCES

1 H.G. Wiedemann and A. Reller, Naturwissenschaften, 79 (1992) 172.
2 A. Oberlin, in P.A. Thrower (Ed.), Chemistry and Physics of Carbon, Vol. 22, Marcel Dekker, New York, 1989, p. 1.
3 S. Amelincks, P. Delavigenette and M. Herschap, in P.L. Walker (Ed.), Chemistry and Physics of Carbon, Vol. 1, Marcel Dekker, New York, 1966 p. 2.
4 F. Atamny, J. Blöcker, A. Dübotzky, H. Kurt, G. Loose, W. Mahdi, O. Timpe and R. Schlögl, J. Mol. Phys., 76, (1992) 851.
5 C. Wong and R.T. Yang, J. Chem. Phys., 78 (1983) 3325.
6 E.L. Evans, R.J.M. Griffiths and J.M. Thomas, Science, 171 (1971) 174.
7 P.L. Walker, Jr., F. Rusinko, Jr. and L.G. Austin, Catal., 11 (1959) 133.
8 F.M. Lang and P. Magnier, in P.L. Walker (Ed.), Chemistry and Physics of Carbon, Vol. 3, Marcel Dekker, New York, 1968, p. 121.
9 U. Göbel, M. Wesemann, W. Bensch and R. Schlögl, Fresnius J. Anal. Chem., 343 (1992) 582.
10 F. Atamny, H. Kollmann, H. Bartl and R. Schlögl, Ultramicroscopy, 48 (1993) 281.
11 F. Atamny, J. Blöcker, B. Henschke, R. Schlögl, Th. Schedel-Niedrig, M. Keil and A.M. Bradshaw, J. Chem. Phys., 96 (1992) 4522.
12 H.P. Boehm and M. Voll, Carbon, 8 (1970) 227.
13 S.S. Barton, D.J. Gillespie and B.H. Harrison, Carbon, 11 (1973) 649.
14 R. Schlögl, G. Loose and M. Wesemann, Solid State Ionics, 43 (1990) 183.
15 B. Stöhr, H.P. Boehm and R. Schlögl, Carbon, 29 (1991) 707.
16 R. Schlögl, Surf. Sci., 189 (1987) 69.
17 P.L. Walker, P.J. Hart, F.J. Vastola, Fundamentals of Gas–Solid Interactions, Academic Press, New York, 1967, p. 307.

18 C. Liu, C. Hsianping and A. Bard, Langmuir, 7 (1991) 1138.
19 H.A. Mices, Sang-il Park and W.A. Harrison, Phys. Rev. B, 36 (1987) 4491.
20 J.B. Pethica, Phys. Rev. Lett., 57 (1986) 3235.
21 F. Atamny, R. Schlögl and W.J. Wirth, Ultramicroscopy, 42 (1992) 660.
22 R. Coratger, A. Claverie, F. Ajustron and J. Beauvillain, Surf. Sci. 227 (1990) 7.
23 H. Marsh and T.E. O'Hair, Carbon, 7 (1969) 702.
24 H. Jüntgen and H. Kühl, in P.A. Thrower (Ed.), Chemistry and Physics of Carbon, Vol. 22, Marcel Dekker, New York, 1989.
25 H. Marsh, N. Mudie, I.A.S. Edwards and H.P. Boehm, in P.A. Thrower (Ed.), Chemistry and Physics of Carbon, Vol. 20, Marcel Dekker, New York, 1987, p. 213.
26 J.M. Thomas, in P.L. Walker (Ed.), Chemistry and Physics of Carbon, Vol 1, Marcel Dekker, New York, 1966, p. 121.
27 A. Kavanagh and R. Schlögl, Carbon, 26 (1988) 23.
28 F. Atamny, R. Schlögl and A. Reller, Carbon, 30 (1992) 1123.